Dry-pressed anodized titania nanotube/$CH_3NH_3PbI_3$ single crystal heterojunctions: the beneficial role of N doping

*Jelena Vujančević [a], Pavao Andričević [b], Anđelika Bjelajac [c], Veljko Đokić [d], Maja Popović [e], Zlatko Rakočević [e], Endre Horváth *[b], Márton Kollár [b], Bálint Náfrádi [b], Andreas Schiller [f], Kondrad Domanski [f], László Forró [b], Vera Pavlović [g], Đorđe Janaćković [d]*

[a] Institute of Technical Sciences of SASA, Knez Mihailova 35/IV, 11000 Belgrade, Serbia

[b] Ecole Polytechnique Fédérale de Lausanne, Laboratory of Physics of Complex Matter (LPMC), CH-1015 Lausanne, Switzerland

[c] University of Belgrade, Innovation Center of Faculty of the Technology and Metallurgy, Karnegijeva 4, 11000 Belgrade, Serbia

[d] University of Belgrade, Faculty of Technology and Metallurgy, Karnegijeva 4, 11000 Belgrade, Serbia

[e] University of Belgrade, Vinča Institute of Nuclear Sciences, Laboratory of Atomic Physics, Mike Alasa 12-14, 11001 Belgrade, Serbia

[f] Fluxim AG, Katharina-Sulzer-Platz 2, CH-8400 Winterthur, Switzerland

[g] University of Belgrade, Faculty of Mechanical Engineering, Kraljice Marije 16, 11000 Belgrade, Serbia

[*]Corresponding author. Tel. +41 21 6934515, Fax. +41 21 6934470, endre.horvath@epfl.ch

ABSTRACT

Highly ordered, anodically grown TiO_2 nanotubes on titanium supports were annealed in ammonia atmosphere in order to incorporate nitrogen doping (< 2 at.%) in the titanium oxide lattice. FESEM micrographs revealed nanotubes with an average outer diameter of 101.5 ± 1.5 nm and an average wall thickness of about 13 nm. Anatase crystals were formed inside the tubes after annealing in ammonia atmosphere for 30 min. With further annealing, rutile peaks appeared due to the thermal oxidation of the foil and rise as the duration of heat treatment was increased. The concentration and chemical nature of nitrogen in the nanotube arrays can be correlated to the optical response of dry-pressed heterojunctions of doped $TiO_2/CH_3NH_3PbI_3$ single crystals. The N-TiO_2/perovskite heterojunction with the highest amount of interstitial nitrogen exhibited an improved photocurrent, indicating the importance of the semiconductor doping-based heterojunction optimization strategies to deliver competitive levels of halide perovskite-based optoelectronic devices to be envisioned for urban infrastructures.

KEYWORDS Annealing in NH_3; titanium dioxide nanotubes; methylammonium lead triiodide photodetectors; optical properties; photocurrent.

1. INTRODUCTION

Great efforts of scientists are focused on enhancing solar energy utilization worldwide. Among the numerous photoactive materials studied, titanium dioxide (TiO_2) has been proven highly promising, since it is chemically stable, cheap, non-toxic and available in abundance. However, in specific applications, such as semiconductor photocatalysis or photodetection, the material faces considerable limitations due to its light absorption edge lying at 387 nm. A significant body of recent research has been focused on extending the effective light absorption range into the visible region.

A key technique for narrowing the band gap of TiO_2 is the incorporation of a dopant atom such as transition metal [1,2] or nonmetal [3–5] in the crystal structure. Among various elements, nitrogen seems to be an appropriate choice, due to its atomic size similar to that of oxygen, small ionization energy and as it is defined by metastable center formation and stability [6]. Many reports have been published about the incorporation of nitrogen into anodized TiO_2 nanotubes by the hydrothermal method [7,8], immersing in nitrogen containing solution [9], ion implantation [10,11], anodization in nitrogen containing electrolyte [12] or thermal treatment in N_2 atmosphere [13], in order to improve the photoelectric or photocatalytic efficiency (Table S1).

Furthermore, several research groups synthesized N-TiO_2 by exposing TiO_2 to hot ammonia gas and studied the influence of the annealing temperature (300 to 600 °C) [14] and the combination of air-ammonia atmosphere [15]. The highest photocurrents were observed in the temperature range of 500-600 °C [14] with mixed, anatase and rutile phase TiO_2 having up to 9 at.% nitrogen incorporated into the lattice [16].

Recently, Bjelajac et al. [17] characterized nitrogen-doped TiO_2 nanotubes decorated with CdS quantum dots for the potential use as a photoanode in quantum dots sensitized solar cells. They anodized the titanium film deposited on FTO glass and annealed it at 450 °C, 30 minutes in NH_3 flow. Analyzed XPS spectra proved the incorporation of nitrogen in the lattice forming $TiO_{2-x}N_x$, with an N:Ti ratio of ~1:100. Consequently, a red-shift from 380 nm to 507 nm was observed.

Unlike the above-listed doping techniques, which require the dopant cation or anion to be part of the hosting lattice, the decoration-based sensitization techniques rely on the creation of new interfaces. Typically, sensitization of the TiO_2 surface can be achieved by depositing different species such as Ag, Au [18], C-N=C, C-NH_2 fragments [19], metal complexes [20], organic dyes [21], quantum dots [22] and organometallic salts [23–25] or coating nanotubes homogenously with a thin layer of light absorber material [26,27]. Recently, the organic-inorganic lead halide perovskites have been introduced as a photosensitizer of titania in various size, form and shape [28]. The frontrunner of this class of materials, methylammonium lead triiodide ($MAPbI_3$) has outstanding optoelectronic properties, such as high absorption coefficient, direct band gap (1.5–1.65 eV) [29], long charge carrier lifetime (9.6 ± 0.3 ns) and electron-hole diffusion length (~100 nm) [30]. Therefore, it shows a great potential to be used in light-emitting diodes [31], lasers [32], solar cells [28], magneto-optical data storage [33], visible light [34,35], X-ray [36] and even high energy particle detection [37]. Most of the aforementioned devices contain polycrystalline thin films that demonstrated limited optical and physical properties due to grain boundaries and higher defect density. Recently, device performance has been improved by using perovskite single crystals. Due to the absence of grain bounders, low

trap densities (~10^{-9}cm^{-3}) and long diffusion lengths (3 mm) which decreases recombination [38,39].

In the majority of these applications, the light-sensitive heterojunctions are formed by interfacing the hybrid perovskite with planar or mesoporous films of titania. The textural properties of the mesoporous films will depend on the size and shape (spherical, tubular, rod or wire) of its nanoparticle building blocks. The nanotubular morphology may offer several advantages over nanoparticles: a 30-fold greater electron diffusion length, reduced charge recombination and faster electron transport, due to which the electron energy loss is reduced [24,40,41]. The anodization technique is frequently used for the synthesis of highly aligned arrays of TiO_2 nanotubes perpendicular to the substrate [42]. A significant body of research suggest that by varying the synthesis parameters and post-synthesis treatments one can control and predict the morphological characteristics and the doping level of TiO_2 nanotubes produced by anodization.

Therefore, our aim is to investigate the influence of the annealing time in ammonia atmosphere on the concentration and chemical nature of nitrogen atoms incorporated in the nanotube arrays. Additionally, we seek to provide answers to whether or not the optical response of dry-pressed heterojunctions of doped $TiO_2/CH_3NH_3PbI_3$ single crystals can be correlated to the amount and chemical nature of nitrogen-dopant incorporated in the TiO_2 nanotube arrays.

2. EXPERIMENTAL SECTION

2.1. Synthesis of undoped and doped TiO_2 nanotubes

Titanium foils (10 mm × 15 mm × 0.25 mm, 99.7 %, Aldrich) were degreased by sonication in acetone, ethanol and deionized water (DI) for 60 min (20 min in each). This was followed by rinsing with DI water and drying in air. The TiO_2 nanotube arrays were synthesized in an electrolyte consisting of 0.6 mM HF and 0.1 mM CH_3COOH in DI water according to the previously reported approach [43]. The electrochemical anodization was carried out in a two-electrode cell using a DC power source (PEQLAB EV 231), where a Ti foil was used as an anode and a thin platinum foil as a counter electrode. The anodization was performed at room temperature, for 30 minutes under 15 V, with mild stirring of the electrolyte. After anodization, the samples were cleaned with DI water and then dried in air. The anodized TiO_2 films were annealed in a quartz tube furnace under an ammonia gas stream (ammonia 3.8, Messer) at 450 °C with a heating rate of 5 °C/min, for 30 min (labeled as TiO_2-N30), 60 min (TiO_2-N60) and 90 min (TiO_2-N90), to introduce different nitrogen quantity. The annealed samples were let to cool down to room temperature under an NH_3 atmosphere. For the pristine sample, the anodized TiO_2 nanotubes were annealed in air at 450 °C for 30 min, with a heating rate of 5 °C/min (designated as TiO_2-undoped). The representative top view image of the undoped-TiO_2 nanotube array annealed in air is presented in Figure 1a.

2.2. The synthesis of methylammonium lead iodide perovskite

For the preparation of perovskite single crystals, the precipitation method was used starting from a concentrated aqueous solution [44] of hydroiodic acid (57 wt% in H_2O, 99.99 % Sigma-Aldrich) containing lead (II) acetate trihydrate (99.99 %, Acros Organics) and a respective amount of a CH_3NH_2 solution (40 wt% in H_2O, Sigma-Aldrich). In order

to induce the saturation of the solute at the low-temperature part of the solution, a constant 55–42 °C temperature gradient was applied. The $MAPbI_3$ crystals were obtained after seven days. An optical image of grey, rhombohedral $MAPbI_3$ single crystals with 3–5 mm silver gray facets is shown in Figure 1b.

2.3. Preparation of TiO_2/$CH_3NH_3PbI_3$ single crystal photodiodes

The heterojunctions were prepared by dry pressing of a bulk, millimeter-sized $MAPbI_3$ single crystal against the surface of TiO_2 and N-TiO_2 nanotubes. Pushed electrical contacts were applied by using tungsten needles. The tungsten needles were contacted with the top part of the $MAPbI_3$ single crystal and titanium plate back-electrode. A schematic representation of the interface and measurement setup can be seen on Figure 1c and d, respectively.

2.4. Characterization

The surface morphology of the TiO_2 nanotube arrays was studied using a Tescan MIRA3 XMU FESEM. The UV–Vis diffusion reflectance spectra were recorded in the wavelength range of 300–800 nm on the Shimadzu UV-2600 spectrophotometer equipped with an integrated sphere. X-ray diffraction patterns were determined by Rigaku Ultima IV diffractometer, in a 2θ range from 23 to 60° with a step size of 0.05° and time of 3 s. Grazing incidence angle was set at 2° to enhance the signal from the film. The X-ray photoelectron spectroscopy was carried out on a SPECS customized UHV surface analysis system containing sputter ion gun, PHOIBOS 100 spectrometer for energy analysis, dual anode Al/Ag monochromatic source and electron flood gun. The XPS spectra were taken

using a monochromatic Al Kα line (photon energy of 1486.74 eV) operated at 400 W. The presented results were obtained after the sputtering of the surface in order to reduce the contribution of atmospheric pollution. The sample sputter cleaning was performed using a 3 keV Ar^+ ion beam, the duration was 1 min in all cases in order to reduce the preferential sputtering effects which typically, in the case of TiO_x samples, reduce 'x'. All binding energies were referenced to the C 1s peak at 284.8 eV of surface adventitious carbon.

2.5. Photodetector device characterization

Two point resistivity measurements (d.c.) were carried out using a National Instruments GPIB-USB-HS controller and a Keithley 2400 source meter. A microscope objective and a micromechanical stage were used to locate the device. A Fiberoptic-Heim LQ 1100 was used as a white light source of 1.83 mW/mm^2. The photocurrent experiments were performed in ambient atmosphere with 30 % relative humidity at 20 °C.

Impendence spectroscopy measurements were carried out using PAIOS 3 (Platform for All-In-One Characterization of Solar Cells and OLED) from Fluxim AG. A voltage signal with frequency swept between 10 MHz and 100 Hz and an amplitude of 70 mV was applied on top of a bias voltage of 0 V. The measurements were performed in the dark and in ambient atmosphere.

3. RESULTS AND DISCUSSION

Halide perovskite crystallites are relatively soft materials [45,46], and, hence efficiently sinter together exposed to a various range of pressures at room temperature. For instance,

Mettan et al. [44] demonstrated that $MASnI_3$ crystallites compressed into pellets allow reliable transport measurements and achieve high ZT values of 0.13 at room temperature. Moreover, Pisoni et al. [47] demonstrated that the resistivity of polycrystalline samples obtained by pressing together an assembly of microcrystallites is only a factor of 2 higher than that of a high-quality single crystal. Even devices, such as perovskite-based photodiodes were recently fabricated by small pressure-assisted mechanical contacts, i.e. by dry pressed perovskite single crystals or pressed pellets on CNT electrodes [35,48]. These mechanically assembled photodiodes detected visible light in the $\mu W/cm^2$ intensity range and exhibit an ideality factor bellow 10. Additionally, pressed pellets have been recently applied to build high-performance X-ray photodetectors [49]. These pioneering works suggest, that the quality pressure-assisted mechanical contacts is surprisingly good, and therefore these type of, so far rarely studied heterojunctions have been used in this work. The heterojunctions were created by dry pressing of a 3 mm $MAPbI_3$ single crystal on top of the undoped and N-doped TiO_2 nanotubes (Figure 1c and d). In order to investigate the effect of N doping on the photodiode performance, the tungsten needles, which served as electrical leads, were pressed on the top surface of the $MAPbI_3$ single crystal and onto the Ti foil back electrode, respectively. Highly ordered nanotubes arrays perpendicular to the Ti foil were obtained during anodization (Figure 1a). To study the morphology evolution during heat treatment in ammonium atmosphere, micrographs were statistically analyzed (Figure S1). It is noteworthy that there was no significant difference in the average pore diameter and the average wall thickness between the nitrogen doped and undoped TiO_2 samples, as can be seen from Table S2. On the other hand, slight differences in outer diameter distribution are observed (Figure S1). A lower Young's modulus [50] of TiO_2

nanotubes compared to TiO_2 films allows the nanotubes to better accommodate the $MAPbI_3$ single crystal, thus leading to larger contact areas. Influence of the annealing atmosphere on the crystal structure of titania nanotubes was followed by XRD measurements. The sample annealed in air for 30 min shows the presence of anatase peaks at ~ 25°, 48° and 55° with a low-intensity peak at 27° for the rutile phase (Figure 2). However, when annealing in an NH_3 atmosphere for 30 min only the anatase phase was visible. With a longer heat treatment of 60 min, the rutile peak appears and increases, while the anatase peaks diminish and broaden. The presence and increase of the rutile phase at 450 °C with increasing time of annealing is probably due to the thermal oxidation of the titanium foil underneath the nanotubes [51,52]. Using the Sherrer's equation [53] $D = 0.9\lambda/d\cos\theta$, where λ is the wavelength of X-ray radiation (1.54 Å), d full width at a half maximum of the peak and θ the diffraction angle, crystals size were calculated and presented in Table S3. A slight increase in anatase crystal size can be observed with longer durations of annealing.

Fig. 1.

Fig. 2.

XPS studies were performed in order to investigate the chemical state of nitrogen incorporated in the TiO_2 structure. Table 1 summarizes the total amount of elements in the samples after sputter cleaning. Because of standard surface contamination, a decrease in the amount of carbon after sputtering was registered for all samples. From Table 1, the titanium foil and TiO_2-undoped sample show a nitrogen peak, just like the samples annealed in NH_3 atmosphere, indicating that the titanium foil contained nitrogen in traces before its exposure

to the NH_3 atmosphere. In order to reveal the nature of nitrogen in the titanium foil, N 1s peak (Figure S2) was deconvoluted in three components: 396.8, 398.8 and 400.6 eV. The peak at 396.8 eV indicates the presence of nitrogen inside the Ti foil because a peak around 396 eV is commonly ascribed to the Ti-N bond. The peak at 398.8 eV is usually associated with Ti-O-N or N-H bond [54], while the peak at 400.6 eV indicates NO species, nitrogen bound to various surface oxygen sites [55]. Therefore, the nitrogen is present inside the foil and on the surface of the foil. On the other hand, the TiO_2-undoped sample showed only two peaks: 399.8 and 401.9 eV, without the peak around 396 eV (Table S4). The peak at 399.7 eV indicates the incorporation of nitrogen in some form into the lattice on interstitial sites [56–59]. Hence, it can be assumed that the peak at 399.8 eV observed in the undoped TiO_2 was due to nitrogen diffusion from the titanium substrate to the TiO_2 nanotubes during the anodization process. The peak around ~401 eV is assigned to molecularly adsorbed nitrogen on the surface of the samples, and it indicates contamination [60]. Finally, for nitrogen-doped TiO_2 samples three N 1s peaks, at ~ 396 eV, ~ 399.7 eV and ~ 401.9 eV, were observed. The binding energy of 396 eV can be attributed to anion N^{3-} that substituted some oxygen site [56,60,61], while the 399.7 and 401.9 eV to interstitial nitrogen and surface contamination, respectively. The total amount of nitrogen decreases with longer heat treatment in ammonia atmosphere, as it is shown in Table 1. Although the nitrogen content decreases, it was observed that the amount of substitutional nitrogen increases (Table S4). This can be due to the fact that a greater amount of nitrogen diffuses from the atmosphere into the structure, resulting in a drop of the concentration gradient of nitrogen with prolonged annealing time. Furthermore, the decreased gradient of concentration is

accompanied by a decreased diffusion from the substrate and a subsequent decrease of the amount of interstitial nitrogen.

In addition, it should not be neglected, that interstitial nitrogen diffuses to substitutional sites with longer exposure to ammonium atmosphere. Thus, the amount of substitution nitrogen increases, while the amount of interstitial nitrogen decreases. Moreover, the amount of chemisorbed nitrogen decreases with prolonged annealing time. Therefore, the total amount of nitrogen becomes lower (Figure 3b).

Table 1

Fig. 3.

In order to determine the influence of nitrogen doping on the optical response of TiO_2, DRS analyses were performed. As evident in Figure 4a, all samples annealed in ammonia atmosphere exhibit a shoulder in the absorption spectra towards higher wavelengths. The same is not present in the pristine sample. The most pronounced increase in absorption is for the TiO_2-N30, which contains the highest proportion of nitrogen. This is presumably caused by introducing new localized states in the band gap of TiO_2 due to nitrogen doping. According to Di Valentin et al. [56] substitutional nitrogen form localized state at 0.14 eV above the valence band edge. While interstitial nitrogen form occupied antibonding states below O2p valance band and bonding states at 0.73 eV above the valence band.

Furthermore, I-V measurements were performed exclusively on the TiO_2 nanotube samples before the addition of perovskite single crystals, to assess whether or not nitrogen doping leads to an increased conductivity as compared to the pristine titanium oxide

nanotubes. The resistivity of both, the pristine and doped samples were comparable and above GΩ approaching the limitations of our two-point resistivity measurement setup. Additionally, impedance spectroscopy measurements confirmed, as seen in Figure 4b, that the conductance of the doped and undoped samples was identical. This suggests that the improved detectivity of the fabricated photodetector devices is not due to the conductivity difference of the TiO_2 electrodes.

Fig. 4.

I-V characteristics for the fabricated heterojunctions of doped and undoped TiO_2 nanotubes with perovskite single crystals are presented in Figure 5a. The measurements were performed at ambient conditions in the dark and under white fluorescent light illumination. All samples were preconditioned by applying a 100 V bias voltage for 75 seconds. As a result, the conductivity of the perovskite crystal increases and stabilizes, giving a constant and comparable signal for all samples (Figure S3). The heterojunctions show diode-like behavior, indicating that a Schottky contact has been formed between the TiO_2 films and the perovskite single crystals. Furthermore, a positive correlation can be observed between the absolute values of the photocurrent and the N-doping. Samples doped with nitrogen show an increased photocurrent as compared to the undoped sample. Nanotubes annealed under ammonium for 30 min exhibit the highest photocurrent. Annealing further decreases the photocurrent achieving almost the photocurrent values of the undoped TiO_2 after 90 minutes. The nature of nitrogen incorporated in the lattice could be the reason for the difference in photoactivity. TiO_2-N30 poses the highest amount of interstitial nitrogen (1.42 at.%) and the lowest amount of substitutional. Whereas, TiO_2-N90 has 0.79 at.% interstitial nitrogen close to the undoped, 0.75 at%. It is an evident

correlation between photocurrent and the amount of interstitial nitrogen. A similar phenomenon was also observed by Cabrera et al. [62]. They synthesized N-TiO_2-films with different amount of interstitial and substitutional nitrogen for photodegradation of stearic aide. An increase in photoactivity was observed for films that contained the highest amount of N_i. Moreover, the film with the lowest level of N_i was the same as the undoped reference sample despite possessing the highest level of N_s. Furthermore, it has been demonstrated that TiO_2 doped with interstitial nitrogen is 30% more photocatalytic active than TiO_2 doped with substitutional nitrogen [63]. This is due to better stability of photo-generated electron-holes in interstitially doped anatase while the tendency for recombination is greater in substitutionally doped samples.

To assure that the increase in photocurrent of the perovskite/TiO_2 device is due to the increase in nitrogen content rather than an increase of O-vacancies, titanium 2p and oxygen 1s core levels were studied. As shown in Table S5, the position of the Ti $2p_{1/2}$ biding energy at 458.8±0.1 eV for undoped and N-doped clearly indicates that Ti is in the 4^+ valence state. There is no decrease in the Ti 2p binding energy after nitrogen doping which could indicate the formation of the Ti^{3+}state (usually in combination with oxygen vacancies). Furthermore, deconvolution of the O 1s peak reveals that all samples have three contributions: 530.1±0.1 eV which proves the O^{2-} state in the crystal lattice; 531.5±0.1 eV attributed to the chemisorbed surface hydroxyl groups; and ~ 532.5 eV which is probably due to weakly adsorbed species [64].

These optoelectronic results are in good agreement with the XPS and DRS analysis. The TiO_2-N30 sample has the highest N_i content and the largest absorbance red shift, which

results in the highest photocurrent. Consequently, with the decrease of interstitial nitrogen content, the optical and electrical characteristics worsen. Furthermore, our results confirm that the amount of interstitial nitrogen is governing the increase of photocurrent. As an example the TiO_2-N90 sample, although possessing a higher substitutional nitrogen content then its TiO_2-N30 counterpart, exhibits lower photocurrent.

Lastly, on-off measurements were done under ambient conditions (Figure 5b). As expected, higher values of photocurrent were achieved using doped TiO_2 nanotubes. In agreement with the I-V measurements, the TiO_2-N30/perovskite device had the best performance, having ~230 % higher photoresponse compared to the undoped reference sample. Typical figures of merit of a photodetector device, the responsivity *R* and response times, t_{rise} and t_{fall}, were calculated. *R* is defined as the ratio of the photocurrent and the intensity of light, while the response times are defined as the times elapsed for the change of the photocurrent intensity from 10 % to 90 % of the peak output photocurrent amplitude. The on-off curves show a fast response regime increasing the current to 75 % of its maximum value. The current then continues to increase, saturating to the final current value. This leads to a rise time of 2.65 s. When the light source is turned off, the decay time is short – 0.33 s. The longer rise time is most probably due to ion migration (pooling) effect in the perovskite single crystal [65], as the measurements were done at relatively high bias voltages. The responsivity for each junction is shown in Figure 5c. Responsivity off the TiO_2-N30 sample is more than double the value for its undoped counterpart. Lastly, the ideality factor of the photodiode was calculated from the I-V measurements and is shown in dependence of the applied voltage in Figure S4.

Fig. 5.

Tian et al. [66] and Ma et al. [67] demonstrated the use of nitrogen-doped TiO_2 electrodes in dye-sensitized solar cells (DSSCs). The formation of O-Ti-N bonds lowers the position of the flat band potential reducing the band gap, which results in the improvement of the open circuit voltage, thus attaining a higher incident photon-to-conversion efficiency. The reason for these enhancements is a new absorption peak in the visible light region between 400 and 550 nm in the nitrogen-doped TiO_2 film. Furthermore, electron transport time and electron lifetime were studied for N-doped TiO_2 and undoped TiO_2 using intensity-modulated photocurrent spectroscopy (IMPS) and intensity modulated photovoltage spectroscopy (IMVS), respectively. Shortening of the electron transport, compared to the electron lifetime, with nitrogen doping, resulted in a higher energy conversion efficiency of the DSSC [68]. Moreover, localized states are formed in the band gap of the metal oxide simultaneously increasing the electron concentration and light absorption efficiency of the DSSC [69]. On the other hand, Zhang et al. [70] studied the influence of nitrogen doping of TiO_2 electron transport layers (ETL) on the performance of perovskite solar cells. They showed that by introducing nitrogen atoms in the structure of TiO_2 nanorods the efficiency of the solar cell increased by 14.7 %, compared to its counterpart using an undoped TiO_2 ETL. In order to explain this, they studied photoluminescence (PL) and time-resolved photoluminescence (TRPL) spectra of undoped $TiO_2/MAPbI_{3-x}Cl_x$ and N-$TiO_2/MAPbI_{3-x}Cl_x$. PL and TRPL spectra showed better electron transfer on the N-$TiO_2/MAPbI_{3-x}Cl_x$ interface than on $TiO_2/MAPbI_{3-x}Cl_x$ interface. In addition, lower resistance and larger recombination resistance of perovskite solar cells based on N-TiO_2 ETL were demonstrated

by electrochemical impedance spectroscopy (EIS). The reason for that is the decreasing of the trap density, due to the lowering of the oxygen vacancies concentration.

Therefore, we believe that the reasons behind the increase of photocurrent and responsivity of the fabricated photodiodes using N-doped TiO_2 nanotube electrodes are in line with the conclusions of these earlier works. Effective electron transfer and lower resistance of the devices with an increase of interstitial nitrogen doping result in better device performance. Future measurements, such as PL, TRPL and EIS could prove these statements and clarify the electron transfer process between the perovskite single crystal and the N-doped TiO_2 nanotube electrodes in detail. Nitrogen-doped TiO_2 nanotube electrodes can, therefore, be attractive as electrodes for future perovskite-based optoelectronic device fabrication.

4. CONCLUSIONS

Well-aligned TiO_2 nanotube arrays were prepared by anodization of titanium foils in an acid electrolyte. Nitrogen doping has been introduced in the titanium oxide nanotubes via high-temperature crystallization in pure NH_3 atmosphere. It has been revealed that the duration of the heat treatment has a direct impact on the amount and nature of the incorporated nitrogen dopant. XPS study demonstrated that nitrogen is incorporated into the nanotubes at both the substitutional and the interstitial sites. The ratios of substitutional and interstitial nitrogen vary as a consequence of diffusion from the titanium substrate and from the ammonia atmosphere as well. Photodiodes have been fabricated by pressing the pristine and N-doped anodized titania nanotubes and millimeter-sized lead methylammonium triiodide single crystals. The photodetectors prepared from the nitrogen-doped samples

annealed at 450 ^{o}C degrees for 30 minutes showed a greatly improved optical response, highlighting the future potential of the semiconductor doping-based (interstitial and substitutional) heterojunction optimization strategies in the development of halide perovskite-based optoelectronic devices.

ACKNOWLEDGMENTS

This research was supported by the Ministry for Science, Education and Technological Development of the Republic of Serbia, project OI 172057 and III 45019 and the Swiss National Science Foundation (No. 160169) and the ERC advanced grant "PICOPROP" (Grant No. 670918). The authors are thankful to Prof. Ion N. Mihailescu, Dr. Gabriel Socol from National Institute for Lasers, Plasma and Radiation Physics, Romania; Dr. Catalin Ducu from the University of Pitesti, Romania for their help, and Dr. Evelyne Knapp for a fruitful discussion on Impedance Spectroscopy.

APPENDIX A. Supplementary material

The supporting information is available free of charge.

REFERENCES

[1] M.M. Momeni, Y. Ghayeb, Fabrication, characterization and photoelectrochemical behavior of Fe–TiO_2 nanotubes composite photoanodes for solar water splitting, J. Electroanal. Chem. 751 (2015) 43–48. doi:10.1016/j.jelechem.2015.05.035.

[2] M.M. Momeni, Y. Ghayeb, Z. Ghonchegi, Fabrication and characterization of copper doped TiO_2 nanotube arrays by in situ electrochemical method as efficient visible-light photocatalyst, Ceram. Int. 41 (2015) 8735–8741.

doi:10.1016/j.ceramint.2015.03.094.

[3] K. Siuzdak, M. Szkoda, M. Sawczak, A. Lisowska-Oleksiak, J. Karczewski, J. Ryl, Enhanced photoelectrochemical and photocatalytic performance of iodine-doped titania nanotube arrays, RSC Adv. 5 (2015) 50379–50391. doi:10.1039/c5ra08407e.

[4] M. Szkoda, A. Lisowska-Oleksiak, K. Siuzdak, Optimization of boron-doping process of titania nanotubes via electrochemical method toward enhanced photoactivity, J. Solid State Electrochem. 20 (2016) 1765–1774. doi:10.1007/s10008-016-3185-8.

[5] M.M. Momeni, Y. Ghayeb, Z. Ghonchegi, Visible light activity of sulfur-doped TiO_2 nanostructure photoelectrodes prepared by single-step electrochemical anodizing process, J. Solid State Electrochem. 19 (2015) 1359–1366. doi:10.1007/s10008-015-2758-2.

[6] D. Lu, M. Zhang, Z. Zhang, Q. Li, X. Wang, J. Yang, Self-organized vanadium and nitrogen co-doped titania nanotube arrays with enhanced photocatalytic reduction of CO_2 into CH_4, Nanoscale Res. Lett. 9 (2014) 272. doi:10.1186/1556-276X-9-272.

[7] L. Sun, J. Cai, Q. Wu, P. Huang, Y. Su, C. Lin, N-doped TiO_2 nanotube array photoelectrode for visible-light-induced photoelectrochemical and photoelectrocatalytic activities, Electrochim. Acta. 108 (2013) 525–531. doi:10.1016/j.electacta.2013.06.149.

[8] S. Hejazi, N. Truong Nguyen, A. Mazare, P. Schmuki, Aminated TiO_2 nanotubes as

a photoelectrochemical water splitting photoanode, Catal. Today. 281 (2017) 189–197. doi:10.1016/j.cattod.2016.07.009.

[9] B. Yuan, Y. Wang, H. Bian, T. Shen, Y. Wu, Z. Chen, Nitrogen doped TiO_2 nanotube arrays with high photoelectrochemical activity for photocatalytic applications, Appl. Surf. Sci. 280 (2013) 523–529. doi:10.1016/j.apsusc.2013.05.021.

[10] X. Hou, F. Liu, K. Yao, H. Ma, J. Deng, D. Li, B. Liao, Photoelectrical properties of nitrogen doped TiO_2 nanotubes by anodic oxidation of N^+ implanted Ti foils, Mater. Lett. 124 (2014) 101–104. doi:10.1016/j.matlet.2014.03.050.

[11] A. Ghicov, J.M. Macak, H. Tsuchiya, J. Kunze, V. Haeublein, L. Frey, P. Schmuki, Ion implantation and annealing for an efficient N-doping of TiO_2 nanotubes, Nano Lett. 6 (2006) 1080–1082. doi:10.1021/nl0600979.

[12] P. Mazierski, M. Nischk, M. Gołkowska, W. Lisowski, M. Gazda, M.J. Winiarski, T. Klimczuk, A. Zaleska-Medynska, Photocatalytic activity of nitrogen doped TiO_2 nanotubes prepared by anodic oxidation: The effect of applied voltage, anodization time and amount of nitrogen dopant, Appl. Catal. B Environ. 196 (2016) 77–88. doi:10.1016/j.apcatb.2016.05.006.

[13] P.H. Le, L.T. Hieu, T.-N. Lam, N.T.N. Hang, N.V. Truong, L.T.C. Tuyen, P.T. Phong, J. Leu, Enhanced photocatalytic performance of nitrogen-doped TiO_2 nanotube arrays using a simple annealing process, Micromachines. 9 (2018) 618. doi:10.3390/mi9120618.

[14] R.P. Vitiello, J.M. Macak, A. Ghicov, H. Tsuchiya, L.F.P. Dick, P. Schmuki, N-Doping of anodic TiO_2 nanotubes using heat treatment in ammonia, Electrochem. Commun. 8 (2006) 544–548. doi:10.1016/j.elecom.2006.01.023.

[15] H. Wang, Y. Yang, J. Wei, L. Le, Y. Liu, C. Pan, P. Fang, R. Xiong, J. Shi, Effective photocatalytic properties of N doped titanium dioxide nanotube arrays prepared by anodization, React. Kinet. Mech. Catal. 106 (2012) 341–353. doi:10.1007/s11144-012-0439-z.

[16] G. Liu, F. Li, D.-W. Wang, D.-M. Tang, C. Liu, X. Ma, G.Q. Lu, H.-M. Cheng, Electron field emission of a nitrogen-doped TiO_2 nanotube array, Nanotechnology. 19 (2008) 025606. doi:10.1088/0957-4484/19/02/025606.

[17] A. Bjelajac, V. Djokić, R. Petrović, N. Bundaleski, G. Socol, I.N. Mihailescu, Z. Rakočević, D. Janaćković, Absorption boost of TiO_2 nanotubes by doping with N and sensitization with CdS quantum dots, Ceram. Int. 43 (2017) 15040–15046. doi:10.1016/j.ceramint.2017.08.029.

[18] I. Paramasivam, J.M. Macak, P. Schmuki, Photocatalytic activity of TiO_2 nanotube layers loaded with Ag and Au nanoparticles, Electrochem. Commun. 10 (2008) 71–75. doi:10.1016/j.elecom.2007.11.001.

[19] R. Beranek, J.M. Macak, M. Gärtner, K. Meyer, P. Schmuki, Enhanced visible light photocurrent generation at surface-modified TiO_2 nanotubes, Electrochim. Acta. 54 (2009) 2640–2646. doi:10.1016/j.electacta.2008.10.063.

[20] Q. Kang, S. Liu, L. Yang, Q. Cai, The photoelectric performances of TiO_2 nanotube arrays-sensitized with organometallic complexes, Anal. Lett. 44 (2011) 1371–1380. doi:10.1080/00032719.2010.512680.

[21] T. Stergiopoulos, A. Valota, V. Likodimos, T. Speliotis, D. Niarchos, P. Skeldon, G.E. Thompson, P. Falaras, Dye-sensitization of self-assembled titania nanotubes prepared by galvanostatic anodization of Ti sputtered on conductive glass, Nanotechnology. 20 (2009) 365601. doi:10.1088/0957-4484/20/36/365601.

[22] Z. Liu, B. Wang, J. Wu, Q. Dong, X. Zhang, H. Xu, Effects of hydroxylation on PbS quantum dot sensitized TiO_2 nanotube array photoelectrodes, Electrochim. Acta. 187 (2016) 480–487. doi:10.1016/j.electacta.2015.11.042.

[23] X. Gao, J. Li, J. Baker, Y. Hou, D. Guan, J. Chen, C. Yuan, Enhanced photovoltaic performance of perovskite $CH_3NH_3PbI_3$ solar cells with freestanding TiO_2 nanotube array films, Chem. Commun. 50 (2014) 6368–6371. doi:10.1039/c4cc01864h.

[24] P. Qin, M. Paulose, M.I. Dar, T. Moehl, N. Arora, P. Gao, O.K. Varghese, M. Grätzel, M.K. Nazeeruddin, Stable and efficient perovskite solar cells based on titania nanotube arrays, Small. 11 (2015) 5533–5539. doi:10.1002/smll.201501460.

[25] R. Salazar, M. Altomare, K. Lee, J. Tripathy, R. Kirchgeorg, N.T. Nguyen, M. Mokhtar, A. Alshehri, S.A. Al-Thabaiti, P. Schmuki, Use of anodic TiO_2 nanotube layers as mesoporous scaffolds for fabricating $CH_3NH_3PbI_3$ perovskite-based solid-state solar cells, ChemElectroChem. 2 (2015) 824–828. doi:10.1002/celc.201500031.

[26] R. Zazpe, H. Sopha, J. Prikryl, M. Krbal, J. Mistrik, F. Dvorak, L. Hromadko, J.M. Macak, A 1D conical nanotubular TiO_2/CdS heterostructure with superior photon-to-electron conversion, Nanoscale. 10 (2018) 16601–16612. doi:10.1039/c8nr02418a.

[27] F. Dvorak, R. Zazpe, M. Krbal, H. Sopha, J. Prikryl, S. Ng, L. Hromadko, F. Bures, J.M. Macak, One-dimensional anodic TiO_2 nanotubes coated by atomic layer deposition: Towards advanced applications, Appl. Mater. Today. 14 (2019) 1–20. doi:10.1016/j.apmt.2018.11.005.

[28] J. Fan, B. Jia, M. Gu, Perovskite-based low-cost and high-efficiency hybrid halide solar cells, Photonics Res. 2 (2014) 111–120. doi:10.1364/PRJ.2.000111.

[29] S.M.H. Qaid, M.S. Al Sobaie, M.A. Majeed Khan, I.M. Bedja, F.H. Alharbi, M.K. Nazeeruddin, A.S. Aldwayyan, Band-gap tuning of lead halide perovskite using a single step spin-coating deposition process, Mater. Lett. 164 (2016) 498–501. doi:10.1016/j.matlet.2015.10.135.

[30] S.D. Stranks, G.E. Eperon, G. Grancini, C. Menelaou, M.J.P. Alcocer, T. Leijtens, L.M. Herz, A. Petrozza, H.J. Snaith, Electron-hole diffusion lengths exceeding 1 micrometer in an organometal trihalide perovskite absorber, Science 342 (2013) 341–344. doi:10.1126/science.1243982.

[31] H. Cho, S.-H. Jeong, M.-H. Park, Y.-H. Kim, C. Wolf, C.-L. Lee, J.H. Heo, A. Sadhanala, N. Myoung, S. Yoo, S.H. Im, R.H. Friend, T.-W. Lee, Overcoming the electroluminescence efficiency limitations of perovskite light-emitting diodes, Science 350 (2015) 1222–1225. doi:10.1126/science.aad1818.

[32] S.A. Veldhuis, P.P. Boix, N. Yantara, M. Li, T.C. Sum, N. Mathews, S.G. Mhaisalkar, Perovskite materials for light-emitting diodes and lasers, Adv. Mater. 28 (2016) 6804–6834. doi:10.1002/adma.201600669.

[33] B. Náfrádi, P. Szirmai, M. Spina, H. Lee, O. V Yazyev, A. Arakcheeva, D. Chernyshov, M. Gibert, L. Forró, E. Horváth, Optically switched magnetism in photovoltaic perovskite $CH_3NH_3(Mn:Pb)I_3$, Nat. Commun. 7 (2016) 13406. doi:10.1038/ncomms13406.

[34] M. Spina, M. Lehmann, B. Náfrádi, L. Bernard, E. Bonvin, R. Gaál, A. Magrez, L. Forró, E. Horváth, Microengineered $CH_3NH_3PbI_3$ nanowire/graphene phototransistor for low-intensity light detection at room temperature, Small. 11 (2015) 4824–4828. doi:10.1002/smll.201501257.

[35] P. Andričević, M. Kollár, X. Mettan, B. Náfrádi, A. Sienkiewicz, D. Fejes, K. Hernádi, L. Forró, E. Horváth, Three-dimensionally enlarged photoelectrodes by a protogenetic inclusion of vertically aligned carbon nanotubes into $CH_3NH_3PbBr_3$ single crystals, J. Phys. Chem. C. 121 (2017) 13549–13556. doi:10.1021/acs.jpcc.7b03421.

[36] B. Náfrádi, G. Náfrádi, L. Forró, E. Horváth, Methylammonium lead iodide for efficient X-ray energy conversion, J. Phys. Chem. C. 119 (2015) 25204–25208. doi:10.1021/acs.jpcc.5b07876.

[37] S. Yakunin, D.N. Dirin, Y. Shynkarenko, V. Morad, I. Cherniukh, O. Nazarenko, D. Kreil, T. Nauser, M. V. Kovalenko, Detection of gamma photons using solution-

grown single crystals of hybrid lead halide perovskites, Nat. Photonics. 10 (2016) 585–589. doi:10.1038/nphoton.2016.139.

[38] Y. Zhang, Y. Liu, Z. Yang, S. (Frank) Liu, High-quality perovskite $MAPbI_3$ single crystals for broad-spectrum and rapid response integrate photodetector, J. Energy Chem. 27 (2018) 722–727. doi:10.1016/j.jechem.2017.11.002.

[39] Q. Dong, Y. Fang, Y. Shao, P. Mulligan, J. Qiu, L. Cao, J. Huang, Electron-hole diffusion lengths > 175 μm in solution-grown $CH_3NH_3PbI_3$ single crystals, Science 347 (2015) 967–970. doi:10.1126/science.aaa5760.

[40] P. Roy, D. Kim, K. Lee, E. Spiecker, P. Schmuki, TiO_2 nanotubes and their application in dye-sensitized solar cells, Nanoscale. 2 (2010) 45–59. doi:10.1039/b9nr00131j.

[41] R.P. Lynch, A. Ghicov, P. Schmuki, A photo-electrochemical Investigation of self-organized TiO_2 nanotubes, J. Electrochem. Soc. 157 (2010) G76–G84. doi:10.1149/1.3276455.

[42] G.K. Mor, O.K. Varghese, M. Paulose, K. Shankar, C.A. Grimes, A review on highly ordered, vertically oriented TiO_2 nanotube arrays: fabrication, material properties, and solar energy applications, Sol. Energy Mater. Sol. Cells. 90 (2006) 2011–2075. doi:10.1016/j.solmat.2006.04.007.

[43] A. Bjelajac, V. Djokic, R. Petrovic, G. Socol, I.N. Mihailescu, I. Florea, O. Ersen, D. Janackovic, Visible light-harvesting of TiO_2 nanotubes array by pulsed laser

deposited CdS, Appl. Surf. Sci. 309 (2014) 225–230. doi:10.1016/j.apsusc.2014.05.015.

[44] X. Mettan, R. Pisoni, P. Matus, A. Pisoni, J. Jaćimović, B. Náfrádi, M. Spina, D. Pavuna, L. Forró, E. Horváth, Tuning of the thermoelectric figure of merit of $CH_3NH_3MI_3$ (M═Pb,Sn) photovoltaic perovskites, J. Phys. Chem. C. 119 (2015) 11506–11510. doi:10.1021/acs.jpcc.5b03939.

[45] M. Spina, A. Karimi, W. Andreoni, C.A. Pignedoli, B. Náfrádi, L. Forró, E. Horváth, Mechanical signatures of degradation of the photovoltaic perovskite $CH_3NH_3PbI_3$ upon water vapor exposure, Appl. Phys. Lett. 110 (2017). doi:10.1063/1.4978687.

[46] L. Ćirić, K. Ashby, T. Abadie, M. Spina, M. Duchamp, B. Náfrádi, M. Kollár, L. Forró, E. Horváth, Mechanical response of $CH_3NH_3PbI_3$ nanowires, Appl. Phys. Lett. 112 (2018). doi:10.1063/1.5023115.

[47] A. Pisoni, J. Jacimovic, B. Náfrádi, P. Szirmai, M. Spina, R. Gaál, K. Holczer, E. Tutis, Metallicity and conductivity crossover in white light illuminated $CH_3NH_3PbI_3$ perovskite, (2016) 1–18. http://arxiv.org/abs/1604.05637.

[48] M. Spina, L. Mihály, K. Holczer, B. Náfrádi, A. Pisoni, L. Forró, E. Horváth, Photodiode response in a $CH_3NH_3PbI_3/CH_3NH_3SnI_3$ Heterojunction, ACS Appl. Mater. Interfaces. 9 (2017) 10198–10202. doi:10.1021/acsami.6b12392.

[49] S. Shrestha, R. Fischer, G.J. Matt, P. Feldner, T. Michel, A. Osvet, I. Levchuk, B. Merle, S. Golkar, H. Chen, S.F. Tedde, O. Schmidt, R. Hock, M. Rührig, M. Göken,

W. Heiss, G. Anton, C.J. Brabec, High-performance direct conversion X-ray detectors based on sintered hybrid lead triiodide perovskite wafers, Nat. Photonics. 11 (2017) 436–440. doi:10.1038/nphoton.2017.94.

[50] G. Crawford, N. Chawla, K. Das, S. Bose, A. Bandyopadhyay, Microstructure and deformation behavior of biocompatible TiO_2 nanotubes on titanium substrate, Acta Biomater. 3 (2007) 359–367. doi:10.1016/j.actbio.2006.08.004.

[51] S.P. Albu, H. Tsuchiya, S. Fujimoto, P. Schmuki, TiO_2 nanotubes - annealing effects on detailed morphology and structure, Eur. J. Inorg. Chem. 2010 (2010) 4351–4356. doi:10.1002/ejic.201000608.

[52] S. Das, R. Zazpe, J. Prikryl, P. Knotek, M. Krbal, H. Sopha, V. Podzemna, J.M. Macak, Influence of annealing temperatures on the properties of low aspect-ratio TiO_2 nanotube layers, Electrochim. Acta. 213 (2016) 452–459. doi:10.1016/j.electacta.2016.07.135.

[53] H. Lin, C.P. Huang, W. Li, C. Ni, S. Shah, Y.-H. Tseng, Size dependency of nanocrystalline TiO_2 on its optical property and photocatalytic reactivity exemplified by 2-chlorophenol, Appl. Catal. B Environ. 68 (2006) 1–11. doi:10.1016/j.apcatb.2006.07.018.

[54] S.A. Al-Thabaiti, R. Hahn, N. Liu, R. Kirchgeorg, S. So, P. Schmuki, S.N. Basahel, S.M. Bawaked, NH_3 treatment of TiO_2 nanotubes: From N-doping to semimetallic conductivity, Chem. Commun. 50 (2014) 7960–7963. doi:10.1039/c4cc02069c.

[55] C. Feng, Y. Wang, Z. Jin, J. Zhang, S. Zhang, Z. Wu, Z. Zhang, Photoactive centers responsible for visible-light photoactivity of N-doped TiO_2, New J. Chem. 32 (2008) 1038–1047. doi:10.1039/b719498f.

[56] C. Di Valentin, E. Finazzi, G. Pacchioni, A. Selloni, S. Livraghi, M.C. Paganini, E. Giamello, N-doped TiO_2: Theory and experiment, Chem. Phys. 339 (2007) 44–56. doi:10.1016/j.chemphys.2007.07.020.

[57] C.W. Dunnill, I.P. Parkin, Nitrogen-doped TiO_2 thin films: photocatalytic applications for healthcare environments, Dalt. Trans. 40 (2011) 1635–1640. doi:10.1039/C0DT00494D.

[58] A.C. Breeson, G. Sankar, G.K.L. Goh, R.G. Palgrave, Rutile to anatase phase transition induced by N doping in highly oriented TiO_2 films, Phys. Chem. Chem. Phys. 18 (2016) 24722–24728. doi:10.1039/c6cp04003a.

[59] C.-W. Wang, W.-D. Zhu, J.-B. Chen, X. Hou, X.-Q. Zhang, Y. Li, J. Wang, F. Zhou, Low-temperature ammonia annealed TiO_2 nanotube arrays: Synergy of morphology improvement and nitrogen doping for enhanced field emission, Thin Solid Films. 556 (2014) 440–446. doi:10.1016/j.tsf.2014.01.066.

[60] R. Asahi, T. Morikawa, T. Ohwaki, K. Aoki, Y. Taga, Visible-light photocatalysis in nitrogen-doped titanium oxides, Science 293 (2001) 269–271. doi:10.1126/science.1061051.

[61] M. Batzill, E.H. Morales, U. Diebold, Influence of nitrogen doping on the defect

formation and surface properties of TiO_2 rutile and anatase, Phys. Rev. Lett. 96 (2006) 026103. doi:10.1103/PhysRevLett.96.026103.

[62] R. Quesada-Cabrera, C. Sotelo-Vazquez, J.A. Darr, I.P. Parkin, Critical influence of surface nitrogen species on the activity of N-doped TiO_2 thin-films during photodegradation of stearic acid under UV light irradiation, Appl. Catal. B Environ. 160–161 (2014) 582–588. doi:10.1016/j.apcatb.2014.06.010.

[63] A. Kafizas, C. Crick, I.P. Parkin, The combinatorial atmospheric pressure chemical vapour deposition (cAPCVD) of a gradating substitutional/interstitial N-doped anatase TiO_2 thin-film; UVA and visible light photocatalytic activities, J. Photochem. Photobiol. A Chem. 216 (2010) 156–166. doi:10.1016/j.jphotochem.2010.06.034.

[64] J.-C. Dupin, D. Gonbeau, P. Vinatier, A. Levasseur, Systematic XPS studies of metal oxides, hydroxides and peroxides, Phys. Chem. Chem. Phys. 2 (2000) 1319–1324. doi:10.1039/a908800h.

[65] H.T. Yi, X. Wu, X. Zhu, V. Podzorov, Intrinsic charge transport across phase transitions in hybrid organo-inorganic perovskites, Adv. Mater. 28 (2016) 6509–6514. doi:10.1002/adma.201600011.

[66] H. Tian, L. Hu, C. Zhang, W. Liu, Y. Huang, L. Mo, L. Guo, J. Sheng, S. Dai, Retarded charge recombination in dye-sensitized nitrogen-doped TiO_2 solar cells, J. Phys. Chem. C. 114 (2010) 1627–1632. doi:10.1021/jp9103646.

[67] T. Ma, M. Akiyama, E. Abe, I. Imai, High-efficiency dye-sensitized solar cell based on a nitrogen-doped nanostructured titania electrode, Nano Lett. 5 (2005) 2543–2547. doi:10.1021/nl051885l.

[68] W. Guo, L. Wu, Z. Chen, G. Boschloo, A. Hagfeldt, T. Ma, Highly efficient dye-sensitized solar cells based on nitrogen-doped titania with excellent stability, J. Photochem. Photobiol. A Chem. 219 (2011) 180–187. doi:10.1016/j.jphotochem.2011.01.004.

[69] M. Motlak, M.S. Akhtar, N.A.M. Barakat, A.M. Hamza, O.-B. Yang, H.Y. Kim, High-efficiency electrode based on nitrogen-doped TiO_2 nanofibers for dye-sensitized solar cells, Electrochim. Acta. 115 (2014) 493–498. doi:10.1016/j.electacta.2013.10.212.

[70] Z.-L. Zhang, J.-F. Li, X.-L. Wang, J.-Q. Qin, W.-J. Shi, Y.-F. Liu, H.-P. Gao, Y.-L. Mao, Enhancement of perovskite solar cells efficiency using N-doped TiO_2 nanorod arrays as electron transfer layer, Nanoscale Res. Lett. 12 (2017) 43. doi:10.1186/s11671-016-1811-0.

FIGURE CAPTIONS

Fig. 1. Schematic illustration of the TiO_2 nanotube array and $MAPbI_3$ single crystal junction: (a) FESEM top view of an undoped TiO_2 nanotube array annealed in air, 450 °C; (b) Image of $MAPbI_3$ single crystals used for the fabrication of photodiodes; (c) Schematic illustration of the interface showing three types of nitrogen doping, N_s substitutional (blue), N_i interstitial (green) and N_{ch} chemisorbed nitrogen (red). Representation of the effect of nitrogen doping on the interface energy diagram; (d) Schematic illustration of the measurement setup.

Fig. 2. XRD patterns of undoped and nitrogen-doped TiO_2 nanotubes on titanium foil (A stands for anatase, R for rutile and Ti for titanium foil).

Fig. 3. (a) Deconvoluted XPS spectra of N 1s core level of the TiO_2 undoped, TiO_2-N30, TiO_2-N60 and TiO_2-N90 (black line-experimental, grey line-background, magenta line-envelope, blue line-substitutional nitrogen, green line-interstitial nitrogen and red line-chemisorbed nitrogen); (b) Concentration of different nitrogen doping versus the time of annealing in ammonia gas.

Fig. 4. (a) UV-vis absorption spectra and (b) Impendence spectroscopy measurements of undoped TiO_2 and nitrogen doped: TiO_2-N30, TiO_2-N60, and TiO_2-N90.

Fig. 5. I-V photocurrent characteristics of TiO_2-$MAPbI_3$ heterojunctions: (a) I-V characteristics in the dark and under visible light (intensity 1.83 mW/mm^2); (b) on-off measurements while applying a bias voltage of 100 V; (c) calculated responsivities.

TABLE CAPTION

Table 1. The total amount of elements after sputter cleaning for Ti foil, TiO_2-undoped, TiO_2-N30, TiO_2-N60, and TiO_2-N90 samples.

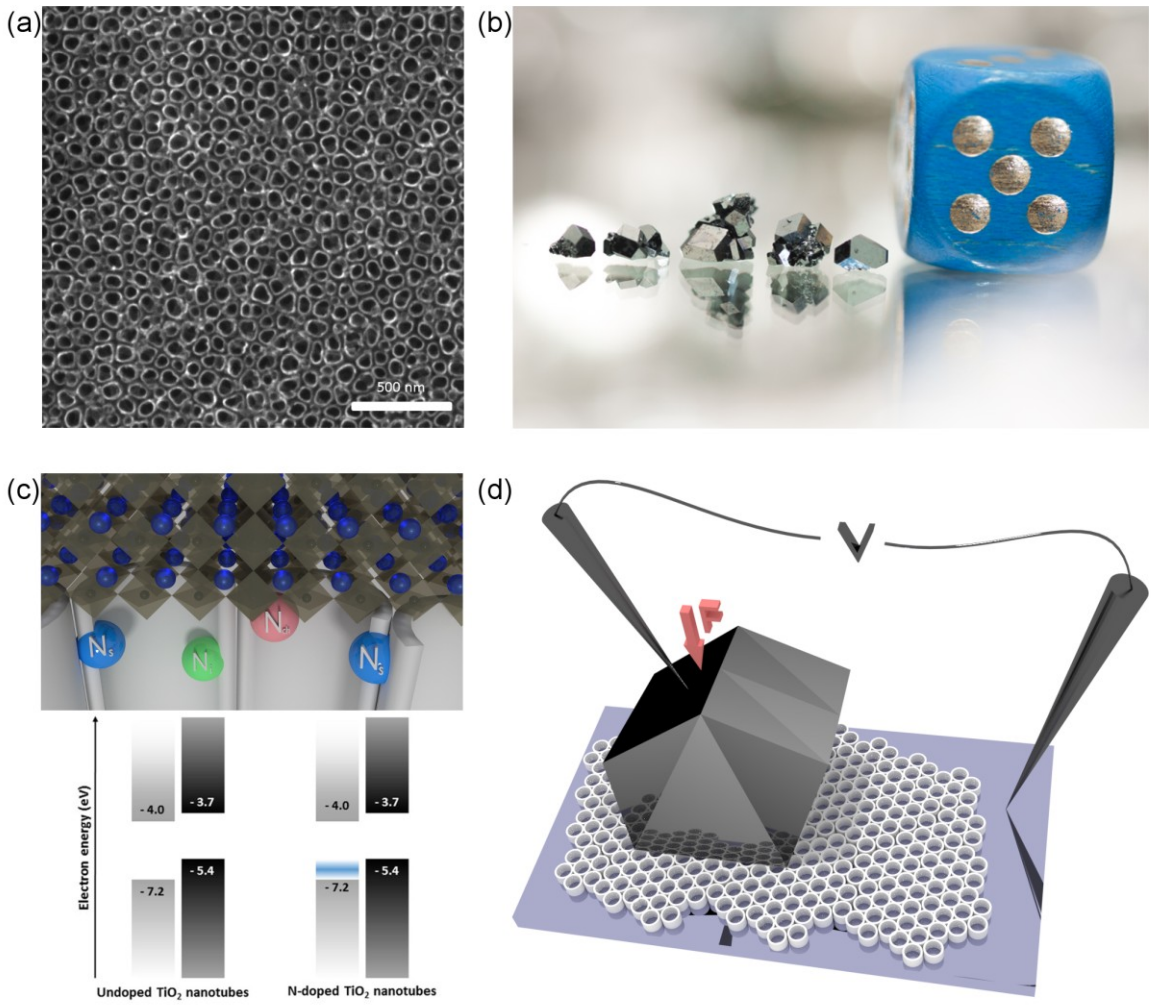
(a)
500 nm
(b)
(c)
N_s
N_i
N_{sc}
N_s
Electron energy (eV)
- 4.0
- 3.7
- 7.2
- 5.4
- 4.0
- 3.7
- 7.2
- 5.4
Undoped TiO_2 nanotubes
N-doped TiO_2 nanotubes
(d)
V
F

Fig. 1.

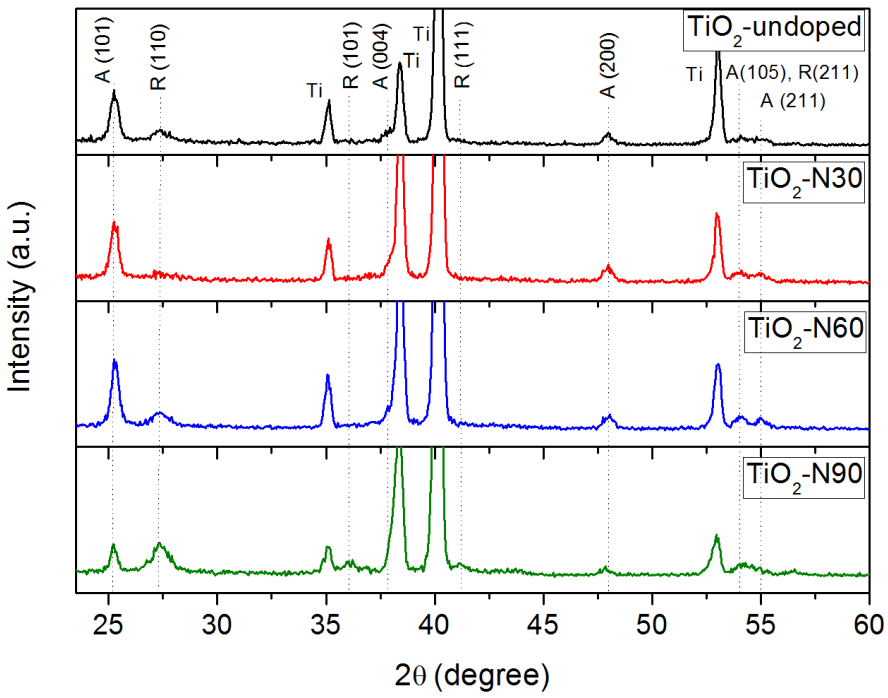
A (101)
R (110)
Ti
R (101)
A (004)
Ti
Ti
R (111)
A (200)
Ti
A(105), R(211)
A (211)
TiO2-undoped
TiO2-N30
TiO2-N60
TiO2-N90
Intensity (a.u.)
25
30
35
40
45
50
55
60
2θ (degree)

Fig. 2.

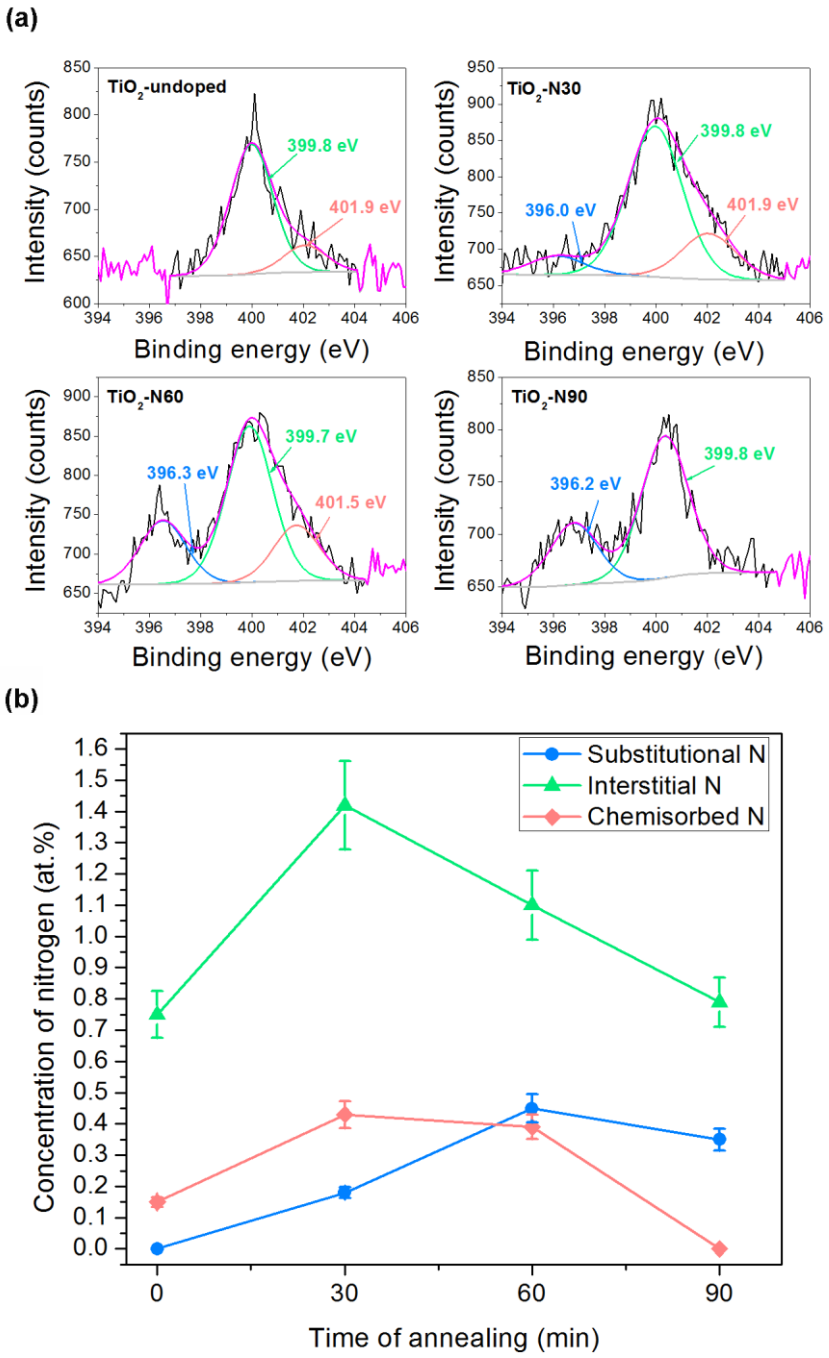
(a)
TiO2-undoped
399.8 eV
401.9 eV
TiO2-N30
396.0 eV
399.8 eV
401.9 eV
TiO2-N60
396.3 eV
399.7 eV
401.5 eV
TiO2-N90
396.2 eV
399.8 eV
Intensity (counts)
Binding energy (eV)
(b)
Substitutional N
Interstitial N
Chemisorbed N
Concentration of nitrogen (at.%)
Time of annealing (min)

Fig. 3.

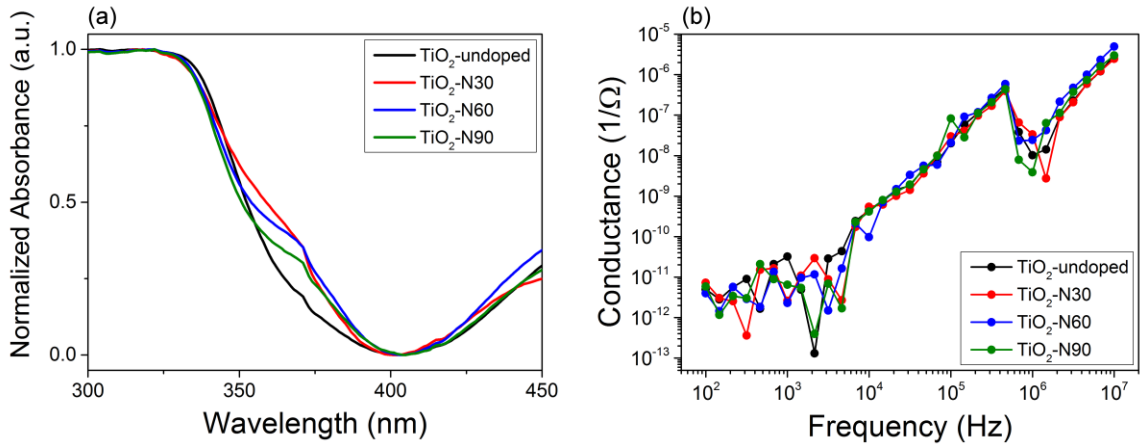
(a)
Normalized Absorbance (a.u.)
Wavelength (nm)
TiO2-undoped
TiO2-N30
TiO2-N60
TiO2-N90
(b)
Conductance (1/Ω)
Frequency (Hz)

Fig. 4.

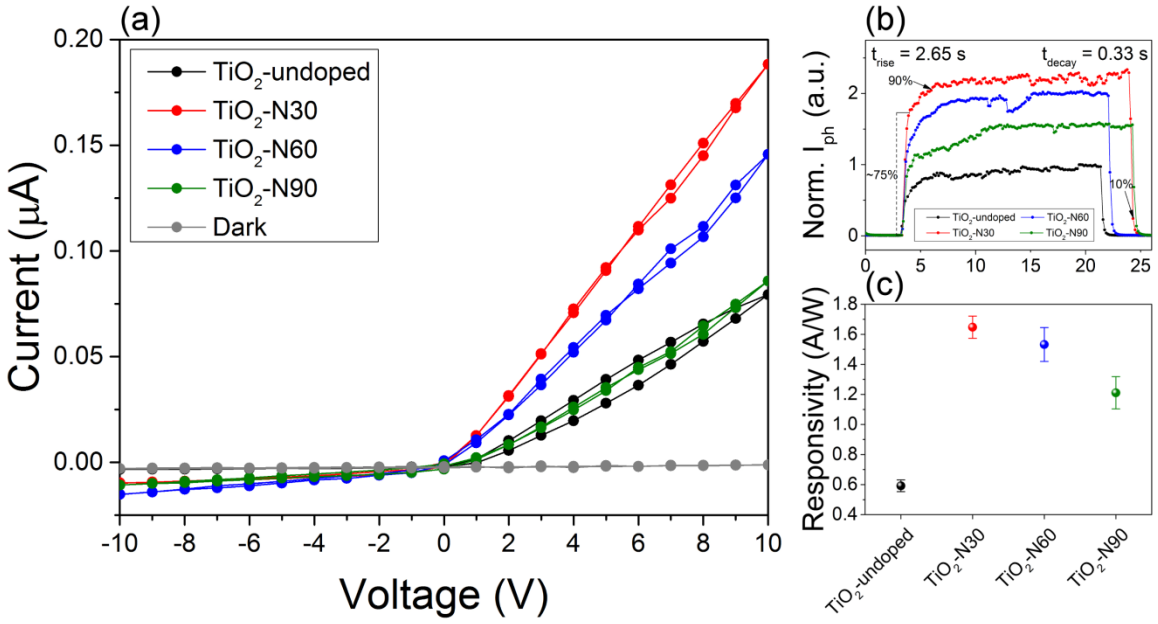
(a)
Current (μA)
Voltage (V)
TiO2-undoped
TiO2-N30
TiO2-N60
TiO2-N90
Dark
(b)
Norm. Iph (a.u.)
trise = 2.65 s
tdecay = 0.33 s
90%
75%
10%
(c)
Responsivity (A/W)

Fig. 5.

Table 1.

Samples	**Ti, at.%**	**O, at.%**	**N, at.%**	**C, at.%**
Ti foil	13.19	47.90	5.40	33.50
TiO_2-undoped	22.53	55.31	0.90	21.26
TiO_2-N30	20.04	54.91	2.03	23.02
TiO_2-N60	20.58	52.10	1.94	25.37
TiO_2-N90	21.86	55.61	1.15	21.39